

TOWARDS REALISTIC NUMERICAL MODELLING OF THIN STRUT-BASED 3D-PRINTED STRUCTURES

Dash, Satabdee;
Nordin, Axel

Lund University

ABSTRACT

The as-built geometry and material properties of parts manufactured using Additive Manufacturing (AM) can differ significantly from the as-designed model and base material properties. These differences can be more pronounced in thin strut-like features (e.g., in a lattice structure), making it essential to incorporate them when designing for AM and predicting their structural behaviour. Therefore, the aim of this study is to develop a numerical model with realistic characteristics based on a thin strut-based test artefact and to use it accurately for estimating its compressive strength. Experiments on test samples produced by selective laser sintering in PA 1101, are used to calculate geometrical deviations, Young's modulus, and yield strength, which are used to calibrate the numerical model. The experimental and numerical results show that the numerical model incorporating geometrical and material deviations can accurately predict the peak load and the force-displacement behaviour. The main contributions of this paper include the design of the test artefact, the average geometrical deviation of the struts, the measured material data, and the developed numerical model.

Keywords: 3D printing, Design for Additive Manufacturing (DfAM), Lattice structures, Computational design methods, Numerical modelling

Contact:

Dash, Satabdee
Lund University
Sweden
satabdee.dash@design.lth.se

Cite this article: Dash, S., Nordin, A. (2023) 'Towards Realistic Numerical Modelling of Thin Strut-Based 3D-Printed Structures', in *Proceedings of the International Conference on Engineering Design (ICED23)*, Bordeaux, France, 24-28 July 2023. DOI:10.1017/pds.2023.360

1 INTRODUCTION

1.1 Background

Additive Manufacturing (AM) has experienced rapid growth in recent years, and for its optimal utilisation, it is essential from an engineering design perspective to understand and incorporate the capabilities and limitations of this technology (Thompson *et al.*, 2016). This integrated practice of designing parts while considering their manufacturing using AM defines the concept of Design for AM or DfAM (Thompson *et al.*, 2016). From a geometrical perspective, implementing the DfAM concept necessitates dimensional characterisation of printed test parts (or artefacts) that replicate specific geometric features (Toguem Tagne *et al.*, 2018). Several studies have been conducted on the development of artefacts by considering DfAM capabilities and limitations (de Pastre *et al.*, 2020). In this paper, we include the design of an AM test artefact that replicates thin strut-like features as often seen in lattice structures for lightweight applications (Xiao *et al.*, 2015).

In general, owing to the manufacturing process, the mechanical characteristics of as-built AM parts can have significant deviations in terms of geometry and material properties (Tkac *et al.*, 2020). To be more precise, there is some geometrical deviation in as-built parts compared to the as-designed (or ideal) computer aided design (CAD) model. Similarly, material properties in as-built parts deviate from the base material(s) they are produced from. These deviations can be even more pronounced in thin strut-based structures (Sindinger *et al.*, 2020), thus making it critical to account for these deviations to accurately predict their structural behaviour.

Finite element (FE) based numerical modelling is a widely adopted technique for predicting the structural behaviour in printed parts. However, in order to improve the prediction accuracy, numerical models with realistic characteristics should be developed to account for deviations due to manufacturing in as-built parts compared to the as-designed parts (Tkac *et al.*, 2020). Therefore, our motivation in this study is to augment the design and analysis of thin strut-based 3D-printed structures by considering deviations due to manufacturing.

1.2 Research aim

To fulfil the research motivation, the specific aim of this paper is to develop a realistic numerical model for predicting the compressive strength of a thin strut-based 3D-printed test artefact. Our aim is based on the hypothesis that such a model can be created by incorporating geometrical and material deviations from the as-built parts within it. The scope of this work is limited to investigating test samples with thin struts of diameter 0.8 mm, manufactured in PA 1101 using selective laser sintering (SLS). Experiments are conducted to investigate their geometrical deviations and compression behaviour. A numerical model is developed to incorporate these deviations obtained from the experimental data. Finally, compressive strength is evaluated in terms of force-displacement response and the peak load of the samples.

1.3 Literature review

The number of numerical and experimental studies investigating the mechanical properties of strut-based lattice structures has significantly increased over the last few years (Karamooz Ravari and Kadkhodaei, 2014; Xiao *et al.*, 2015; Tancogne-Dejean *et al.*, 2016; Gautam *et al.*, 2018; Kummert *et al.*, 2021). Several studies have been involved in predicting the mechanical properties without calibrating the numerical models from the experimental analysis of printed structures (Park *et al.*, 2014; Al-Saedi *et al.*, 2018; Xia *et al.*, 2022). However, given the significance of a realistic numerical model, the focus has been recently shifting towards incorporating experimental data from the printed structures, for example, geometrical deviations and material properties into the numerical models (Gorgularslan *et al.*, 2015; Tkac *et al.*, 2020). Vrana *et al.* (2022) have experimentally investigated and numerically incorporated the shape and dimensional differences in lattices manufactured in an aluminium alloy using selective laser melting (SLM). They aimed at predicting their stress-strain response. On the other hand, Iyibilgin *et al.* (2013) adopted an inverse numerical modelling approach that includes numerical models with variable cross-section struts for sandwich lattices to represent material build-up phenomena in AM. Dallago *et al.* (2018) studied the geometrical differences and defects in lattices printed in a titanium alloy using SLM and developed FE models to predict the

elastic modulus. While also focusing on geometrical deviations, [Gorguluarslan *et al.* \(2015\)](#) developed a numerical model at varying scales for implementing material characterisation in the form of Young's modulus from experimentation of lattices printed in ABS using fused deposition modelling (FDM). Similarly, [Tkac *et al.* \(2020\)](#) conducted compression tests on strut-based lattice composites printed in ABS using FDM to experimentally derive a material model for FE-based prediction of their damage behaviour. However, to the authors' knowledge, none of the studies have focused on developing a realistic numerical model to investigate the compressive strength of thin strut-based structures manufactured in PA 1101 using SLS.

2 METHODOLOGY

The methodology adopted in this work is presented in Figure 1 and further detailed in subsections 2.1 to 2.3.

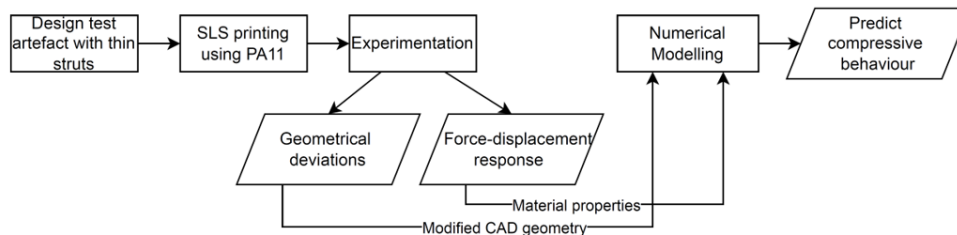


Figure 1: Methodology adopted in the research work

2.1 Design and fabrication

To validate the hypothesis stated in Section 1.2, a test artefact with thin struts was designed and manufactured using AM.

2.1.1 Geometric modelling of test artefact

The test artefact was designed to include 8 cylindrical struts of 7 mm height and 0.8 mm diameter joining two circular discs of diameter 15.3 mm and thickness 1 mm. To achieve uniform distribution of loads during compression, the diameter of these discs was dimensioned to match the force sensor attachment (Figure 4a), and to ensure symmetrical loading, they were designed to be circular. Rhinoceros 3D along with Grasshopper 3D, an integrated visual programming language, was used to perform the geometrical CAD modelling of the designed artefact as shown in Figure 2.

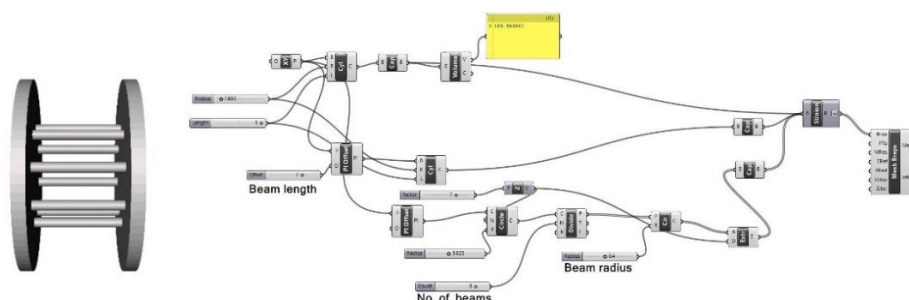


Figure 2: Geometric modelling of test artefact in Rhino-Grasshopper interface

2.1.2 Additive manufacturing of test artefact

To understand the geometrical deviations and their effects on the behaviour of the 3D-printed thin struts, six samples (and dummy samples) of the test artefact were manufactured using SLS technology on a Formiga P110 machine (EOS GmBH, Germany). PA 1101, a bio-based polyamide powder, was employed as the base material. The material properties are listed in Table 1. The manufacturing process parameters used for SLS printing are listed in Table 2.

Table 1. Properties of PA 1101 (EOS GmBH)

Material	Density	Young's modulus	Poisson's ratio	Yield strength	Melting temperature
PA1101	990 kg/m ³	1600 MPa	0.4	48 MPa	201 (20 ^o /min) °C

Table 2. Manufacturing process parameters

SLS parameters	Laser type	Laser power	Laser scan speed	Laser hatch spacing	Powder layer thickness	Powder bed temperature
Values	CO ₂ 1060 nm	25 W	5000 mm/s	0.25 mm	0.1 mm	185° C

To fix the effects of print orientation, the struts were oriented horizontally, i.e., on the XY plane in Figure 3 which is considered favourable according to earlier studies on print orientation (Dash and Nordin, 2022). This orientation also prevents any interlayer effects. To avoid additional effects due to positioning, these samples were placed at the centre and 20 mm apart from each other along the X and Y axes on the printer build plate (see Figure 3). After the printing was done, an air jet cleaning was carefully employed for the removal of loose powder from the samples.

2.2 Experimentation

2.2.1 Geometrical measurements

To understand the geometrical deviations in the test samples, experiments were set up to perform dimensional measurements. To distinguish the test samples from each other, they were numbered sequentially from S1 to S6 (S7 and S8 are dummy samples) based on their position on the build plate (see Figure 3). Each sample was marked 'L' on the left circular disc near the topmost strut (namely Strut 1) in the print orientation shown in Figure 2. This is done to distinguish the left and right sides and to identify Strut 1. Geometrical measurements were made using digital vernier callipers in a clockwise sequence, beginning with Strut 1. This was done to ensure that the measurements are recorded for the same strut across all the samples. Measurements were recorded at the left (1 mm from edge), middle (3.5 mm from either edges), and right portions (1 mm from edge) for each strut contributing to 24 measurements from 8 struts in each sample. This is done to record the dimensional variation along the height of the cylindrical struts.

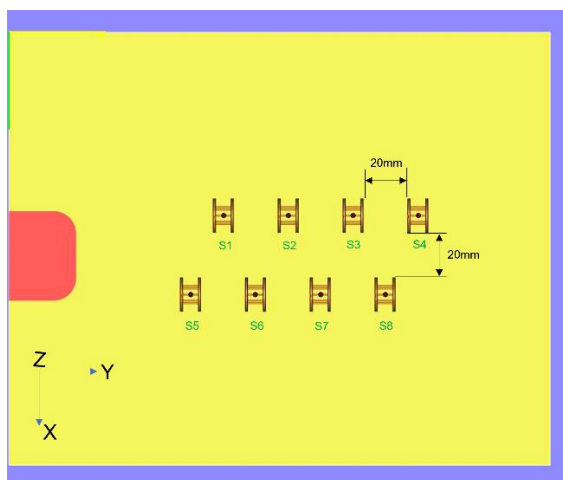


Figure 3: Positioning of test samples (plus dummy samples) on printer build plate

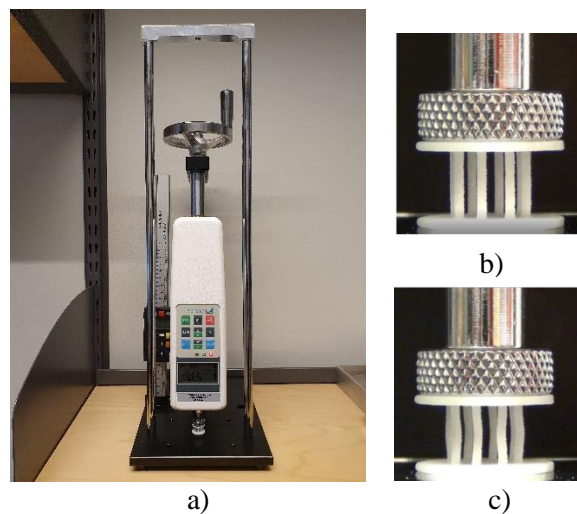


Figure 4: a) Force gauge with test stand for compression test b) Sample 4 before compression c) Sample 4 after compression

2.2.2 Compression tests

To understand the compressive behaviour of the test samples, an experimental setup with SAUTER manual test stand (Sauter GmbHa) employing a digital force gauge SAUTER FH 100 (Sauter GmbHb) (maximum range 100 N, resolution 0.05 N) with a digital length meter was used to perform uniaxial compression tests. The experimental setup has been presented in Figure 4a. Prior to conducting the experiments, the stiffness of the test stand was calculated by gradually compressing the force gauge against the base of the test stand. Thereafter, calibration and preliminary compression tests were performed on the dummy samples (S7, S8). The *before* and *after* compression stages for sample 4 are shown in Figure 4b, 4c. The displacement loads were applied with gradual increments of 0.01

mm until 0.6 mm and the readings on the force gauge and the length meter display were recorded for each sample.

After the compression tests were performed, the displacement recordings from the length meter display were corrected by considering the test stand stiffness calculated previously. The force-displacement curves from these corrected readings were plotted using MATLAB to graphically present the compressive behaviour of each sample. The slope of the region between 10-40 N was used to calculate Young's modulus and calibrate the yield strength for the samples.

2.3 Numerical model

The numerical model was developed to replicate the experimental setup and capture the force-displacement response. The model was created in ANSYS Workbench and consisted of three steps: 1) an initial static structural analysis with a small load of 0.01 mm, 2) a linear eigenmode buckling analysis pre-stressed from the initial analysis, and 3) a non-linear static structural analysis with perturbations from the buckling analysis and a displacement load of 0.5 mm. The purpose of adding perturbations was to replicate the geometric deviations in the printed parts. Without these imperfections, the buckling load would be overestimated (Haynie and Hilburger, 2010; Castro *et al.*, 2014). The Young's modulus and yield strength were determined from the experiments as previously described in Section 2.2.2 and are reported in Section 3.2.

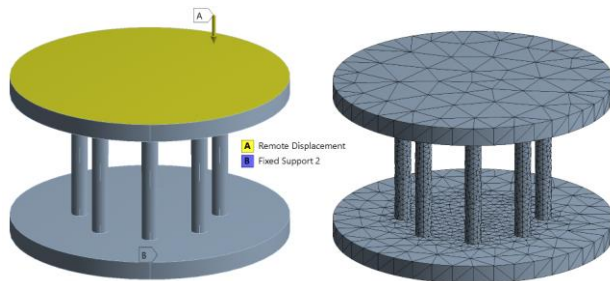


Figure 5: From left to right: Displacement load and constraint, mesh

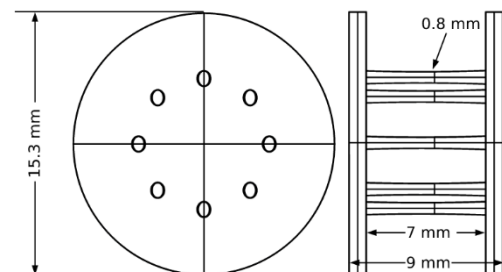


Figure 6: CAD models with measurements from experimental data.

For simplification, a perfectly plastic isotropic hardening material model was used for the numerical model. For the struts, meshing was performed using solid 3D elements with a mesh size of 0.3 mm. The first analysis was performed with a small, forced displacement of the top plate (i.e., the plate facing the force gauge in the experiment) with a fixed support on the bottom plate (see Figure 5). In the buckling analysis, the first 15 buckling modes were determined and used as the basis for displacement perturbations in the non-linear analysis. Multiple modes were used since the buckling mode observed in the experiments may not correspond to the lowest one in the numerical analysis due to the geometrical deviations and/or material defects. For the perturbed structural analysis, the displacement values from the buckling analysis were normalized between 0 and 0.075 mm, which is the average measured deviation of the strut diameters between the CAD model and test samples as reported in Section 4. The normalized displacements were applied as initial displacements for each node using the ANSYS command *upgeom*. The *Large deflection* option was set to ON, the initial and minimum sub-steps were set to 50 with the *Weak springs* option being set to OFF.

2.3.1 Modelling of samples based on experimental data

To include the measured geometrical deviations in the numerical model, the samples with the lowest and highest recorded peak loads were modelled in CAD (see Figure 6) using the measured diameters reported in Table 4. The modelling is based on the assumptions that the struts are elliptical, that all struts in each sample are identical, and that the thickness of the struts varies continuously along their length. The models were created in Rhino-Grasshopper by creating three elliptical cross-sections for the strut - at the left, middle, and right sides with diameters based on the measurements reported in Table 3. A loft was then created for a continuous connection of these cross-sections.

3 RESULTS

3.1 Experimental results

The results from the geometrical measurements and compression tests on the samples are presented in Sections 3.1 to 3.3.

3.1.1 Geometrical results

The geometrical measurements recorded for all the test samples are presented in Table 3.

Table 3. Geometrical measurements (in mm) for test samples

#	Average strut diameters along struts								Average diameter across struts		
	Strut 1	Strut 2	Strut 3	Strut 4	Strut 5	Strut 6	Strut 7	Strut 8	Left	Mid	Right
#1	0.74	0.78	0.88	0.89	0.72	0.78	0.88	0.87	0.82	0.74	0.81
#2	0.74	0.78	0.88	0.89	0.72	0.78	0.88	0.87	0.83	0.75	0.85
#3	0.77	0.79	0.90	0.84	0.73	0.80	0.89	0.86	0.84	0.77	0.84
#4	0.75	0.81	0.90	0.84	0.75	0.78	0.90	0.83	0.83	0.76	0.86
#5	0.74	0.80	0.88	0.78	0.72	0.80	0.89	0.85	0.82	0.76	0.83
#6	0.74	0.77	0.86	0.86	0.75	0.81	0.88	0.88	0.83	0.74	0.86

The individual strut diameters for the middle portions of the struts in each sample are plotted on a radar chart as shown in Figure 7. The radar chart is limited to the middle portions to avoid any edge effects on the results due to the transition of geometry at the strut ends. The expanding rings represent strut diameters in ascending order, ranging from 0 to 1 with an increment of 0.2 mm. The markings on the outermost ring represent Strut 1 to 8 as numbered in Table 3.

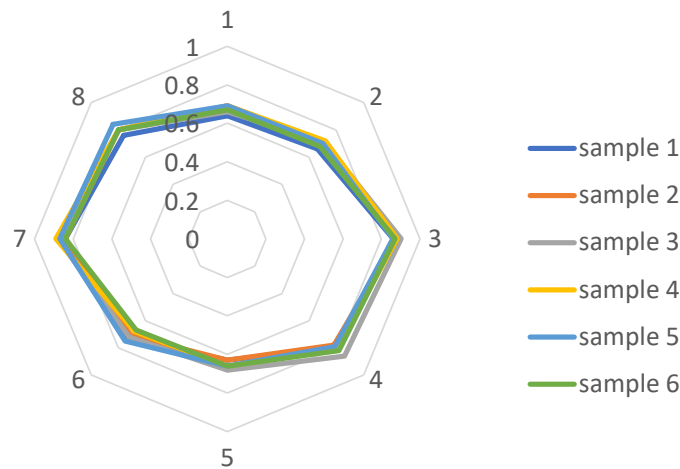


Figure 7: Radar chart comparing strut diameters for each sample

3.1.2 Compression test results

The force-displacement curves for all the test samples obtained from the compression tests are plotted in MATLAB and presented graphically in Figure 8. The peak load variation for the test samples is less than 15% between the maximum (68.5 N) and minimum (59.8 N) values. The linear region investigated in this study, ranges from 10 to 40 N and is represented by the dotted black lines as seen in Figure 8. For the recordings in this region, a built-in curve fitting tool in MATLAB is used to perform curve fitting using linear models. The average stiffness obtained from the fitted curves is 474 N/mm which results in a Young's modulus of 950 MPa.

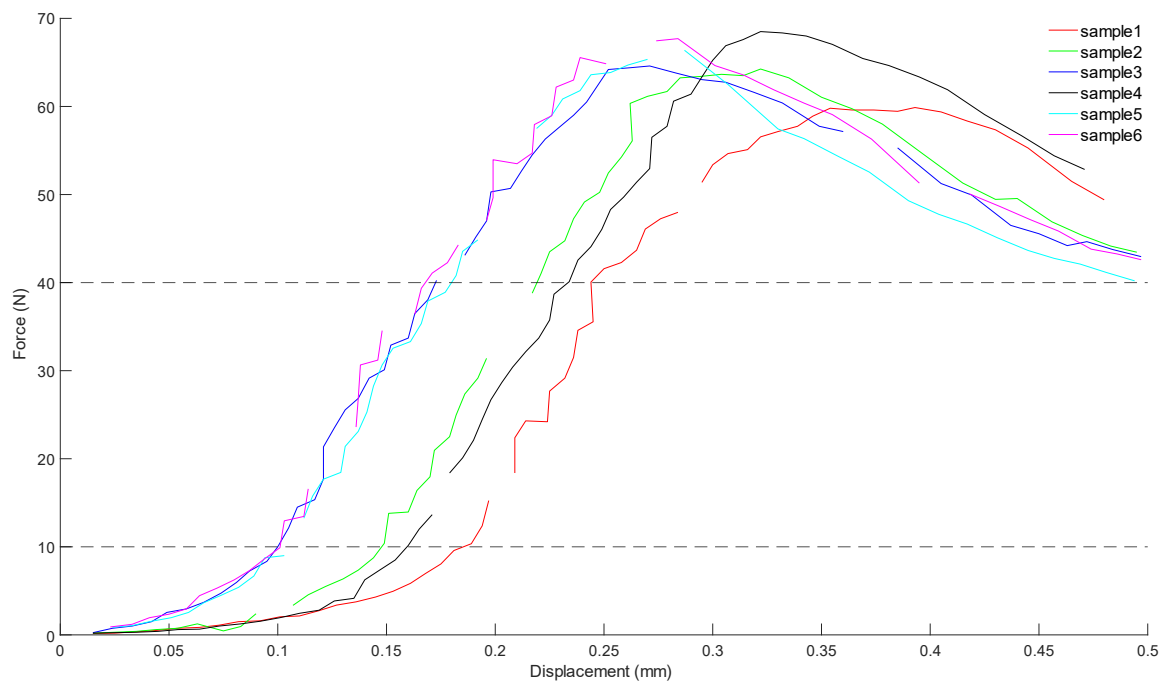


Figure 8: Force - displacement curves illustrating the compressive behaviour of test samples

3.2 Numerical results

Based on the experimental data, Young's modulus was set to 950 MPa and the yield strength was calibrated to 42 MPa. The samples with the lowest and highest peak load (sample 1 and 4) were modelled according to the dimensions in Table 4 and compared to the ideal CAD model with and without added perturbations as described in Section 2.3. The resulting deformation at the peak load and at the full 0.5 mm displacement is shown in Figure 9.

Table 4. Strut diameters (in mm) of the samples with the highest and lowest peak load

Sample	Left min	Left max	Mid min	Mid max	Right min	Right Max
Sample 1	0.72	0.87	0.63	0.86	0.78	0.89
Sample 4	0.82	0.92	0.66	0.89	0.78	0.89

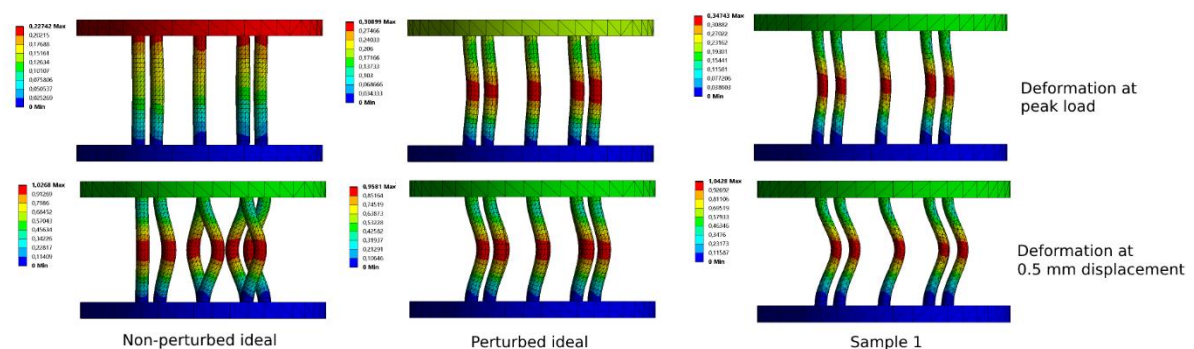


Figure 9: Deformation results at peak load and 0.5 mm displacement

3.3 Comparison between experimental and numerical results

The experimental and numerical results for samples 1 and 4 are combinedly plotted in MATLAB and presented graphically in Figure 10. For comparison, the numerical results for ideal CAD geometry against the perturbed CAD geometry are also presented in the same plot. To enable a comparison of the experimental and numerical results, all the curves were shifted to maintain a zero displacement when the force is 10 N. This is done by using the built-in linear interpolation function, *interp* in MATLAB.

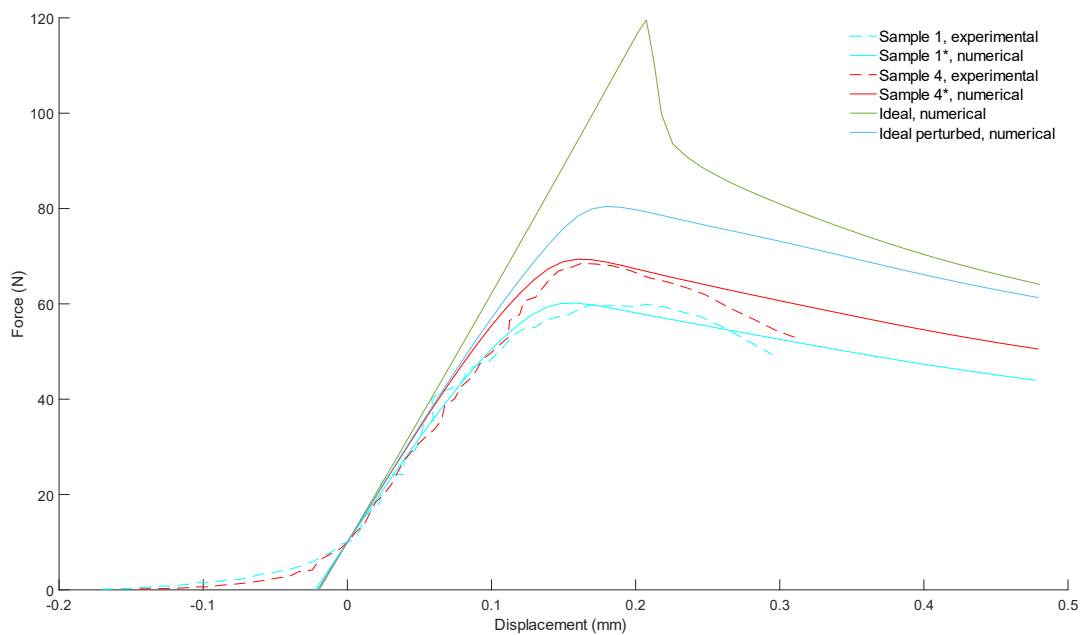


Figure 10: Force - displacement curves comparing the compressive behaviour of test samples obtained from experimentation and numerical simulations

The peak load obtained in each of the force-displacement curves in Figure 10 has been presented in Table 5. In all the result cases, the maximum equivalent stress values at the peak load indicated plastic deformation.

Table 5. Experimental and numerical results for maximum force (numerical with *)

Result (N)	Sample 1	Sample 1*	Sample 4	Sample 4*	Nonperturbed ideal	Perturbed ideal
Peak load	59.88	60.19	68.50	69.37	119.58	80.44

4 DISCUSSION

Tapered strut geometry: The geometrical measurements in Table 3 demonstrate that the printed struts are non-identical and have non-uniform cylindricity. By comparing the average diameters across struts, it is observed that the middle of the struts (Mid values in Table 3) has a lower diameter than the ends (Left and Right values in Table 3). This results due to a difference in material deposition along the height of the struts compared to their ends, which is caused by the transition of the geometry and due to the printing technique.

Elliptical strut cross-section: The radar chart in Figure 7 exhibits a distinct elliptical pattern when the strut diameters for all samples are considered. Across all the samples, minimum diameter is observed for struts 1 and 5 while the maximum diameter is observed for struts 3 and 7. One of the probable reasons is the elliptical cross sections of the printed struts caused by the layering effect. This assumption is consistent with the research findings by [Vrana et al. \(2022\)](#) and [Dallago et al. \(2018\)](#).

Design tolerance: Considering all test samples, the average measured deviation of the strut diameters between the CAD model and test samples is 0.075 mm, indicating design tolerances to be considered. This deviation is around 9% of the as-designed strut diameter of 0.8 mm, thus demonstrating the importance of taking geometrical deviations into account in case of thin struts.

Force-displacement response: The force-displacement curves in Figure 8 indicate similar compressive behaviour in the linear region (10-40 N). As stated in Section 3.1.2, the calculated experimental value of Young's modulus is 950 MPa which is significantly lower in comparison to 1600 MPa for the base material PA 1101. Some of the probable reasons for the observed difference include moisture absorption by samples at room temperature due to their high surface-to-volume ratio ([Salazar et al., 2014](#)) or the printing process influencing Young's modulus in thin struts ([Sindinger et al., 2020](#)). As seen in Figure 10, the force-displacement curves predicted by the numerical model are in good agreement with the experimental data until the peak load is reached. The numerical and experimental curves diverge after the peak load since the chosen material model limits the investigation post-onset of plastic deformations.

Peak load: The results in Table 5 show that the peak load predicted by the numerical model is in good agreement with the experimental data. The difference between the numerical and experimental data for samples 1 and 4 is 0.5% and 1.3%, respectively. The comparison of samples 1 and 4 in Tables 4 and 5 show that the differences in peak load between samples can be predicted by variations in strut diameters. The importance of taking geometrical deviations into account is demonstrated by comparing the peak load of sample 4 to the ideal geometry, which overestimates the peak load by 17.4%. This importance is further emphasised by the peak load variation (< 15%) across the samples which indicates the margin of safety. The effects of adding perturbations to mimic the geometrical deviations can be seen by comparing the peak load of the ideal geometry with and without perturbations, where the nonperturbed model overestimates the peak load by 48.7%.

5 CONCLUSIONS AND FUTURE WORK

The motivation behind this work is to augment the design and analysis of thin strut-based 3D-printed structures by considering deviations due to manufacturing. To expand the knowledge within this area, this paper presents a realistic numerical model for predicting the compressive strength of a thin strut-based 3D-printed test artefact by incorporating geometrical and material deviations into the model. The paper presents experimental and numerical results from the investigation of six test samples printed in PA 1101 using SLS.

The findings reflect the importance of modelling the geometric and material characteristics of as-printed parts to accurately predict their compressive strength. The experimental results on geometrical deviation show that the as-printed struts have a tapered geometry with an elliptical cross-section. The average strut diameter values indicate the design tolerance that should be considered in the ideal CAD model. The experimental results on material deviation from the compression tests show that the as-printed part possess a different Young's modulus and yield strength than the base material. The experimental and numerical results confirm that the numerical model developed using these geometrical and material deviation data can be used to accurately predict the peak load and force-displacement response up until the peak load values. Therefore, the numerical model presented in this paper as well as the geometrical and material data should be applicable to the design and analysis of similar thin strut-based structures in the future. The design of the test artefact should also allow for calibrating the model for alternative materials, processes, and/or strut sizes.

To conclude, the results of this research revealed the importance of a realistic numerical model and demonstrate the possibility of obtaining accurate results with a relatively simple numerical model and test equipment. However, this research is currently delimited to only one material, one process, one strut diameter, and one print orientation. Therefore, further research is needed to assess the applicability of the model by varying these parameters. Additionally, there has been no attempt to experimentally capture the local stress-strain strut behaviour, nor to accurately model the samples' behaviour after the onset of plasticity. Therefore, further research using more samples is planned in future.

ACKNOWLEDGMENTS

This work was financially supported by the MISTRA Foundation (Swedish Foundation for Strategic Environmental Research) through STEPS (Sustainable Plastics and Transition Pathways) project.

REFERENCES

- Al-Saedi, D. S. J., Masood, S. H., Faizan-Ur-Rab, M., Alomarah, A. and Ponnusamy, P. (2018), "Mechanical properties and energy absorption capability of functionally graded F2BCC lattice fabricated by SLM", *Materials & Design*, Vol. 144, pp. 32-44. <https://doi.org/10.1016/j.matdes.2018.01.059>.
- Castro, S. G. P., Zimmermann, R., Arbelo, M. A., Khakimova, R., Hilburger, M. W. and Degenhardt, R. (2014), "Geometric imperfections and lower-bound methods used to calculate knock-down factors for axially compressed composite cylindrical shells", *Thin-Walled Structures*, Vol. 74, pp. 118-132. <https://doi.org/10.1016/j.tws.2013.08.011>.
- Dallago, M., Zanini, F., Carmignato, S., Pasini, D. and Benedetti, M. (2018), "Effect of the geometrical defectiveness on the mechanical properties of SLM biomedical Ti6Al4V lattices", *Procedia Structural Integrity*, Vol. 13, pp. 161-167. <https://doi.org/10.1016/j.prostr.2018.12.027>.
- Dash, S. and Nordin, A. (2022), "Effects of print orientation on the design of additively manufactured bio-based flexible lattice structures", *DS 118: Proceedings of NordDesign 2022*, Design Society, pp. 1-12. <https://doi.org/10.35199/NORDDDESIGN2022.13>

- de Pastre, M.-A., Toguem Tagne, S.-C. and Anwer, N. (2020), "Test artefacts for additive manufacturing: A design methodology review", *CIRP Journal of Manufacturing Science and Technology*, Vol. 31, pp. 14-24. <https://doi.org/10.1016/j.cirpj.2020.09.008>.
- EOS GmbHa. "Formiga P 110 Velocis SLS machine". [online]. Available at: <https://www.eos.info/en/additive-manufacturing/3d-printing-plastic/eos-polymer-systems/formiga-p-110-velocis> (accessed 15/11/2022).
- EOS GmbHb. "PA 1101 Material datasheet". [online]. Available at: <https://www.eos.info/en/additive-manufacturing/3d-printing-plastic/sls-polymer-materials/pa-11-nylon-abs-pa6> (accessed 15/11/2022).
- Gautam, R., Idapalapati, S. and Feih, S. (2018), "Printing and characterisation of Kagome lattice structures by fused deposition modelling", *Materials & Design*, Vol. 137, pp. 266-275. <https://doi.org/10.1016/j.matdes.2017.10.022>.
- Gorgularslan, R. M., Park, S.-I., Rosen, D. W. and Choi, S.-K. (2015), "A multilevel upscaling method for material characterization of additively manufactured part under uncertainties", *Journal of Mechanical Design*, Vol. 137 No. 11, p. 111408. <https://doi.org/10.1115/1.4031012>.
- Haynie, W. and Hilburger, M. W. (2010), "Comparison of methods to predict lower bound buckling loads of cylinders under axial compression", Collection of Technical Papers - AIAA/ASME/ASCE/AHS/ASC Structures, *Structural Dynamics and Materials Conference*. <https://doi.org/10.2514/6.2010-2532>.
- Iyibilgin, O., Yigit, C. and Leu, M. C. (2013), "Experimental investigation of different cellular lattice structures manufactured by fused deposition modeling", *24th International Solid Freeform Fabrication Symposium*, Austin, TX, USA, 2013, pp. 895-907.
- Karamooz Ravari, M. R. and Kadkhodaei, M. (2014), "A computationally efficient modeling approach for predicting mechanical behavior of cellular lattice structures", *Journal of Materials Engineering and Performance*, Vol. 24 No. 1, pp. 245-252. <https://doi.org/10.1007/s11665-014-1281-4>.
- Kummert, C., Schmid, H.-J., Risse, L. and Kullmer, G. (2021), "Mechanical characterization and numerical modeling of laser-sintered TPE lattice structures", *Journal of Materials Research*, Vol. 36 No. 16, pp. 3182-3193. <https://doi.org/10.1557/s43578-021-00321-3>.
- Park, S.-i., Rosen, D. and Duty, C. (2014), "Comparing mechanical and geometrical properties of lattice structure fabricated using Electron Beam Melting", *2014 Annual International Solid Freeform Fabrication Symposium - An Additive Manufacturing Conference*, Austin, TX, USA, 6 Aug 2014, Vol. 1, pp. 1359-1370.
- Salazar, A., Rico, A., Rodríguez, J., Segurado Escudero, J., Seltzer, R. and Martin de la Escalera Cutillas, F. (2014), "Monotonic loading and fatigue response of a bio-based polyamide PA11 and a petrol-based polyamide PA12 manufactured by selective laser sintering", *European Polymer Journal*, Vol. 59, pp. 36-45. <https://doi.org/10.1016/j.eurpolymj.2014.07.016>.
- Sauter GmbHa. "Instruction Manual SAUTER TVL series". [online]. Available at: <https://docs.rs-online.com/6664/0900766b81686e53.pdf> (accessed 29/11/2022).
- Sauter GmbHb. "Digital force gauge FH-S". [online]. Available at: <https://www.kern-sohn.com/shop/de/messinstrumente/kraftmessgeraete/FH-S/> (accessed 29/11/2022).
- Sindinger, S.-L., Kralovec, C., Tasch, D. and Schagerl, M. (2020), "Thickness dependent anisotropy of mechanical properties and inhomogeneous porosity characteristics in laser-sintered polyamide 12 specimens", *Additive Manufacturing*, Vol. 33, p. 101141. <https://doi.org/10.1016/j.addma.2020.101141>.
- Tancogne-Dejean, T., Spierings, A. B. and Mohr, D. (2016), "Additively-manufactured metallic micro-lattice materials for high specific energy absorption under static and dynamic loading", *Acta Materialia*, Vol. 116, pp. 14-28. <https://doi.org/10.1016/j.actamat.2016.05.054>.
- Thompson, M. K., Moroni, G., Vaneker, T., Fadel, G., Campbell, R. I., Gibson, I., Bernard, A., Schulz, J., Graf, P., Ahuja, B. and Martina, F. (2016), "Design for additive manufacturing: trends, opportunities, considerations, and constraints", *CIRP Annals - Manufacturing Technology*, Vol. 65 No. 2, pp. 737-760. <https://doi.org/10.1016/j.cirp.2016.05.004>. English.
- Tkac, J., Samborski, S., Monkova, K. and Debski, H. (2020), "Analysis of mechanical properties of a lattice structure produced with the additive technology", *Composite Structures*, Vol. 242, p. 112138. <https://doi.org/10.1016/j.compstruct.2020.112138>.
- Toguem Tagne, S.-C., Rupal, B. S., Mehdi-Souzani, C., Qureshi, A. J. and Anwer, N. (2018), "A Review of AM Artifact Design Methods", *euspens ASPE Summer Tropical Meeting on Advancing Precision in Additive Manufacturing*, Berkeley, CA, USA, 22-25 July 2018.
- Vrana, R., Koutecky, T., Cervinek, O., Zikmund, T., Pantelejev, L., Kaiser, J. and Koutny, D. (2022), "Deviations of the SLM Produced Lattice Structures and Their Influence on Mechanical Properties", *Materials*, Vol. 15 No. 9, p. 3144. <https://doi.org/10.3390/ma15093144>.
- Xia, H., Meng, J., Liu, J., Ao, X., Lin, S. and Yang, Y. (2022), "Evaluation of the Equivalent Mechanical Properties of Lattice Structures Based on the Finite Element Method", *Materials*, Vol. 15 No. 9, p. 2993. <https://doi.org/10.3390/ma15092993>.
- Xiao, L., Song, W., Wang, C., Liu, H., Tang, H. and Wang, J. (2015), "Mechanical behavior of open-cell rhombic dodecahedron Ti-6Al-4V lattice structure", *Mater. Sci. Eng. A*, Vol. 640, pp. 375-384. <https://doi.org/10.1016/j.msea.2015.06.018>.